

Chiral Dynamics and S-wave contributions in Semileptonic D_s/B_s decays into $\pi^+\pi^-$

Yu-Ji Shi¹ *, and Wei Wang^{1,2} †

¹ INPAC, Shanghai Key Laboratory for Particle Physics and Cosmology,
Department of Physics and Astronomy, Shanghai Jiao-Tong University, Shanghai, 200240, China

² State Key Laboratory of Theoretical Physics, Institute of Theoretical Physics,
Chinese Academy of Sciences, Beijing 100190, China

In this work, we study the semileptonic decay modes $B_s^0 \rightarrow \pi^+\pi^-\ell^+\ell^-$ and $D_s^+ \rightarrow \pi^+\pi^-\ell^+\nu$ in the kinematics region where the $\pi^+\pi^-$ system has a invariant mass in the range 0.5-1.3 GeV. These processes are valuable towards the determination of S-wave $\pi^+\pi^-$ light-cone distribution amplitudes whose normalizations are scalar form factors. We compare the results for scalar form factors predicted in unitarized chiral perturbation theory and extracted from the data on the $B_s \rightarrow J/\psi\pi^+\pi^-$. Then the $B_s \rightarrow \pi^+\pi^-$ and $D_s \rightarrow \pi^+\pi^-$ form factors are calculated in light-cone sum rules, based on which predictions for differential decay widths are made. The results are in good agreement with the experimental data on the B_s and D_s decays into $\pi^+\pi^-$. More accurate measurements at BEPC, LHC and KEKB in future will be helpful to examine our formalism and constrain the input parameters more precisely.

I. INTRODUCTION

It is anticipated that new physics (NP) beyond the standard model (SM) can be indirectly probed through the precision exploration of low-energy processes. An ideal platform is to study the flavor-changing neutral current (FCNC). Rare B decays like the $b \rightarrow s\ell^+\ell^-$, with tiny decay probabilities in the SM, are sensitive to NP degrees of freedom and thus can be exploited as indirect searches of these unknown effects. In terms of observables ranging from the decay probabilities, forward-backward asymmetries, polarizations to a full angular analysis, the exclusive decay mode $B \rightarrow K^*\ell^+\ell^-$ can provide us with a wealth of information on weak interactions. Recent measurements of the almost form-factor independent ratio P'_5 by the LHCb collaboration have indicated a deviation from the SM by about 3.7σ [1, 2].

In fact, the $B \rightarrow K^*\ell^+\ell^-$ is a four-body decay process since the K^* meson is reconstructed in the $K\pi$ final state. Thus it is more appropriate to explore the $B \rightarrow M_1M_2\ell^+\ell^-$, in which various partial-waves of M_1M_2 contribute [3–5]. The S-wave contributions to $B \rightarrow K\pi\ell^+\ell^-$ have been discussed for instance in Refs. [6–12]. The bottom mass m_b is much heavier than the hadronic scale Λ_{QCD} , which allows an expansion of the hard-scattering kernels in terms of the strong coupling constant α_s and the power-scaling parameter Λ_{QCD}/m_b . On the other side, final state interactions among the two-light hadrons should be constrained by unitarity and analyticity. A formalism that makes use of these two advantages has been developed in Refs. [12–14], and summarized in Ref. [15]. Such an approach was pioneered in Ref. [16, 17], and a method without the analysis of hard-scattering kernels has been explored recently in Refs. [18–23]. See also Refs. [24–27] for attempts to analyze charmless three-body B decays. The aim of this work is to further examine this formalism by confronting the theoretical results with the relevant data on $B_s \rightarrow \pi^+\pi^-\mu^+\mu^-$ and $D_s \rightarrow \pi^+\pi^-e^+\nu_e$.

In Ref. [28], the LHCb collaboration has performed an analysis of rare B_s decays into the $\pi^+\pi^-\mu^+\mu^-$ final state with the measured branching ratio:

$$\mathcal{B}(B_s \rightarrow \pi^+\pi^-\mu^+\mu^-) = (8.6 \pm 1.5 \pm 0.7 \pm 0.7) \times 10^{-8}, \quad (1)$$

* Email: shiyuji@sjtu.edu.cn

† Email: wei.wang@sjtu.edu.cn

where the errors are statistical, systematic and arise from the normalization, respectively. The dominant contribution is the $B_s \rightarrow f_0(980)\mu^+\mu^-$ [28]:

$$\mathcal{B}(B_s \rightarrow f_0(980)(\rightarrow \pi^+\pi^-)\mu^+\mu^-) = (8.3 \pm 1.7) \times 10^{-8}. \quad (2)$$

This has triggered theoretical interpretations based on two-meson light-cone distribution amplitudes (LCDAs) [29, 30].

Previously, the CLEO collaboration has investigated the $D_s \rightarrow \pi^+\pi^-\ell\nu_e$, in which the $f_0(980)$ contribution is found dominant as well [31, 32]

$$\mathcal{B}(D_s \rightarrow f_0(980)(\rightarrow \pi^+\pi^-)e^+\nu_e) = (2.0 \pm 0.3 \pm 0.1) \times 10^{-3}. \quad (3)$$

A recent analysis based on the CLEO-c data [33] gives a similar result

$$\mathcal{B}(D_s \rightarrow f_0(980)(\rightarrow \pi^+\pi^-)e^+\nu_e) = (1.3 \pm 0.2 \pm 0.1) \times 10^{-3}. \quad (4)$$

The BES-III collaboration will collect about $2fb^{-1}$ data in e^+e^- collision at the energy around 4.17GeV, which will be used to study semileptonic and nonleptonic D_s decays [34].

The rest of this paper is organized as follows. In Sec. II, we will give the results for scalar $\pi\pi$ form factors and the non-local LCDAs. Sec. III will be devoted to the calculation of the $B_s \rightarrow \pi^+\pi^-$ and $D_s \rightarrow \pi^+\pi^-$ form factors in the light-cone sum rules (LCSR). In Sec. IV, phenomenological results for a variety of observables in the $B_s \rightarrow \pi^+\pi^-\ell^+\ell^-$, $B_s \rightarrow \pi^+\pi^-\nu\bar{\nu}$ and $D_s \rightarrow \pi^+\pi^-\ell\nu$ are presented, and compared to the experimental data if available. An agreement between theory and data will be shown in this section. Our conclusions will be given in Sec. V.

II. SCALAR $\pi^+\pi^-$ FORM FACTORS AND S-WAVE LCDAS

A. Scalar form factor

We start with the definition of a scalar form factor:

$$\langle \pi^+\pi^- | \bar{s}s | 0 \rangle = B_0 F_{\pi\pi}^s(m_{\pi\pi}^2), \quad (5)$$

and the B_0 is the QCD condensate parameter:

$$\langle 0 | \bar{q}q | 0 \rangle \equiv -f_\pi^2 B_0, \quad (6)$$

with f_π as the leading order (LO) pion decay constant. For the numerics, we use $f_\pi = 91.4\text{MeV}$ and $\langle 0 | \bar{q}q | 0 \rangle = -[(0.24 \pm 0.01)\text{GeV}]^3$ [35]. This corresponds to $B_0 = (1.7 \pm 0.2)\text{GeV}$.

In the literature, a variety of approaches have been used to calculate the $F_{\pi\pi}^s(m_{\pi\pi}^2)$, including the (unitarized) chiral perturbation theory (χ PT) [36–43] and dispersion relations [44]. In the χ PT, the LO and next-to-leading order (NLO) results can describe the low-energy data with a good accuracy, but with the increase of the invariant mass, higher-order contributions become more important. This is under expectation since the perturbative expansion in χ PT is organized in terms of $p_\pi/(4\pi f_\pi)$. It has been argued that the unitarized approach, by summing higher order corrections, can extend the χ PT applicability to the scale around 1 GeV [45]. A fit to the BES data on the $\pi\pi$ invariant mass distributions in $J/\psi \rightarrow \pi^+\pi^-\phi$ [46] has been performed in this approach and an overall agreement is found [39]. The fitted result for $F_{\pi\pi}^s(m_{\pi\pi}^2)$ is shown in Fig. 1. The modulus, real part and imaginary part are shown as solid, dashed and dotted curves, from which one can observe the broad structure for the $\sigma(600)$ and the peak at $f_0(980)$ is naturally produced.

In recent years the LHCb collaboration has conducted a series of analyses of angular distributions in the $B_s \rightarrow J/\psi\pi^+\pi^-$ decay mode [47, 48]. In this procedure, the S-wave contributions have been explicitly separated, and three resonances, $f_0(980)$, $f_0(1500)$ and $f_0(1790)$, have been identified. To access the $\pi^+\pi^-$ invariant mass distribution,

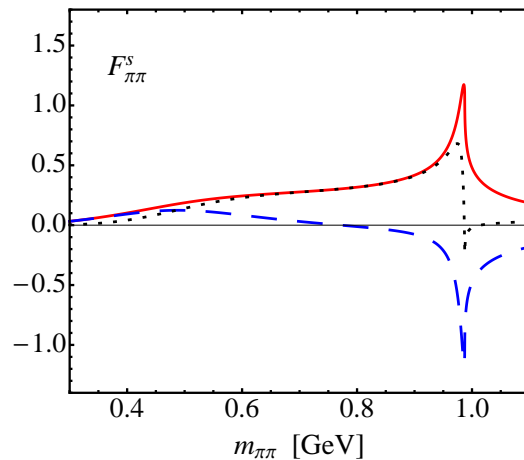


FIG. 1: The $F_{\pi\pi}^s(m_{\pi\pi}^2)$ in unitarized χ PT. The modulus, real part and imaginary part are shown in solid, dashed and dotted curves. The result is based on the fit of the BES data on the $\pi\pi$ invariant mass distributions in $J/\psi \rightarrow \pi^+\pi^-\phi$ [46] in Ref. [39].

the Breit-Wigner formula is employed for the $f_0(1500)$ and $f_0(1790)$. Due to the fact that the $f_0(980)$ lies in the vicinity of the $K\bar{K}$ threshold, the Flatté model [49, 50] has been adopted. Considering the relative strengths and strong phases among different resonances, we have

$$\begin{aligned}
 F_{\pi\pi}^s(m_{\pi\pi}^2) = & \frac{c_1 m_{f_0(980)}^2 e^{i\theta_1}}{m_{\pi\pi}^2 - m_{f_0(980)}^2 + im_{f_0(980)}(g_{\pi\pi}\rho_{\pi\pi} + g_{KK}F_{KK}^2\rho_{KK})} \\
 & + \frac{c_2 m_{f_0(1500)}^2 e^{i\theta_2}}{m_{\pi\pi}^2 - m_{f_0(1500)}^2 + im_{f_0(1500)}\Gamma_{f_0(1500)}(m_{\pi\pi}^2)} \\
 & + \frac{c_3 m_{f_0(1790)}^2 e^{i\theta_3}}{m_{\pi\pi}^2 - m_{f_0(1790)}^2 + im_{f_0(1790)}\Gamma_{f_0(1790)}(m_{\pi\pi}^2)}. \tag{7}
 \end{aligned}$$

The $\rho_{\pi\pi}$ and ρ_{KK} are phase space factors [47, 48, 50]:

$$\rho_{\pi\pi} = \frac{2}{3}\sqrt{1 - \frac{4m_{\pi^\pm}^2}{m_{\pi\pi}^2}} + \frac{1}{3}\sqrt{1 - \frac{4m_{\pi^0}^2}{m_{\pi\pi}^2}}, \quad \rho_{KK} = \frac{1}{2}\sqrt{1 - \frac{4m_{K^\pm}^2}{m_{\pi\pi}^2}} + \frac{1}{2}\sqrt{1 - \frac{4m_{K^0}^2}{m_{\pi\pi}^2}}. \tag{8}$$

Compared to the normal Flatté distribution, an additional correction has been introduced in the LHCb fit above the $K\bar{K}$ threshold to better describe the data [48]

$$F_{KK} = \exp(-\alpha k^2), \tag{9}$$

where k is the kaon momentum in the $K\bar{K}$ rest frame, and α is set to $\alpha = 2.0\text{GeV}^{-2}$ [48]. The energy-dependent width $\Gamma_S(m_{\pi\pi}^2)$ for an S -wave resonance is parameterized as

$$\Gamma_S(m_{\pi\pi}^2) = \Gamma_S \frac{m_S}{m_{\pi\pi}} \left(\frac{m_{\pi\pi}^2 - 4m_\pi^2}{m_S^2 - 4m_\pi^2} \right)^{\frac{1}{2}} F_R^2, \tag{10}$$

with the constant width Γ_S , and the Blatt-Weisskopf barrier factor $F_R = 1$ [48]. The c_i and θ_i , $i = 1, 2$, and 3, are tunable parameters. In the fit by LHCb, two solutions are found and the fitted parameters for three contributing components are collected in Tab. I [48].

In Fig. 2, we compare the results for the scalar form factor calculated in the unitarized χ PT (dashed curve), and the ones extracted from the $B_s \rightarrow J/\psi\pi^+\pi^-$ data based on Eq. (7) (solid and dotted curves). The constant c_1 in Eq. (7) has been tuned in the comparison. The two solutions found by the LHCb give very similar shapes as shown in the figure. There are a few remarks on the shapes.

TABLE I: Fitted parameters for contributing components in the $B_s \rightarrow J/\psi\pi^+\pi^-$ by the LHCb collaboration [48]. Two solutions are found in the fit.

Fractions (%)	Solution I	Solution II
$f_0(980)$	$70.3 \pm 1.5^{+0.4}_{-5.1}$	$92.4 \pm 2.0^{+0.8}_{-16.0}$
$f_0(1500)$	$10.1 \pm 0.8^{+1.1}_{-0.3}$	$9.1 \pm 0.9 \pm 0.3$
$f_0(1790)$	$2.4 \pm 0.4^{+5.0}_{-0.2}$	$0.9 \pm 0.3^{+2.5}_{-0.1}$
Phase differences ($^\circ$)	Solution I	Solution II
$f_0(1500) - f_0(980)$	138 ± 4	177 ± 6
$f_0(1790) - f_0(980)$	78 ± 9	95 ± 16
Parameter	Solution I	Solution II
$m_{f_0(980)}$ (MeV)	945.4 ± 2.2	949.9 ± 2.1
$g_{\pi\pi}$ (MeV)	167 ± 7	167 ± 8
$g_{\kappa\kappa}/g_{\pi\pi}$	3.47 ± 0.12	3.05 ± 0.13
$m_{f_0(1500)}$ (MeV)	1460.9 ± 2.9	1465.9 ± 3.1
$\Gamma_{f_0(1500)}$ (MeV)	124 ± 7	115 ± 7
$m_{f_0(1790)}$ (MeV)	1814 ± 18	1809 ± 22
$\Gamma_{f_0(1790)}$ (MeV)	328 ± 34	263 ± 30

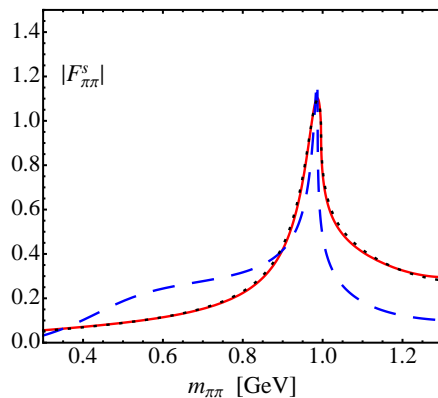


FIG. 2: The $F_{\pi\pi}^s(m_{\pi\pi}^2)$ predicted in the χ PT (dashed curve), and fitted from the $B_s \rightarrow J/\psi\pi^+\pi^-$ data (solid line for solution and dotted line for solution II). The two fitted solutions are not distinguishable below 1.2 GeV.

- On the contrary with the χ PT results, the parametrization in Eq. (7) does not contain the $f_0(500)$ (or the so-called σ) contribution. The LHCb collaboration has set an upper limit for the ratio [48]:

$$R = \frac{F_r(f_0(500))}{F_r(f_0(980))} < 0.3\% \quad (11)$$

at a 90% C.L.

- The expansion parameter in χ PT is $p_\pi/(4\pi f_\pi)$, where the p_π is the pion's momentum. Summing higher order s-channel contributions and incorporating the coupled channel effects will extend the applicability region up to 1 GeV. On the other hand, the parametrization in Eq. (7) has explicitly included two scalar resonances, $f_0(1500)$ and $f_0(1790)$, and thus is valid in the region above 1 GeV.
- At the $f_0(980)$, the unitarized χ PT leads to a very narrow peak. This feature is smeared out in the data since the binned results for the $\pi\pi$ invariant mass distributions are presented on the experimental side. Still the parametrization in Eq. (7) is well consistent with the data on the $B_s \rightarrow J/\psi\pi^+\pi^-$ [47, 48].

- From the comparison, we can see that at the current stage the advantages in both cases are not overwhelming. In future, we hope the results can be improved in some more sophisticated methods like the unitarized approach with resonances [40]. In the following, we will use the parametrization form inspired by the data in Eq. (7).

B. Generalized LCDAs

With the scalar form factor as the normalization condition, the S-wave $\pi^+\pi^-$ LCDAs are defined by [12, 51–54]:

$$\begin{aligned}\langle(\pi^+\pi^-)_S|\bar{s}(x)\gamma_\mu s(0)|0\rangle &= F_{\pi\pi}^s(m_{\pi\pi}^2)p_{\pi\pi,\mu}\int_0^1 du e^{iup_{\pi\pi}\cdot x}\phi_{\pi\pi}(u), \\ \langle(\pi^+\pi^-)_S|\bar{s}(x)s(0)|0\rangle &= F_{\pi\pi}^s(m_{\pi\pi}^2)B_0\int_0^1 du e^{iup_{\pi\pi}\cdot x}\phi_{\pi\pi}^s(u), \\ \langle(\pi^+\pi^-)_S\bar{s}(x)\sigma_{\mu\nu}s(0)|0\rangle &= -F_{\pi\pi}^s(m_{\pi\pi}^2)B_0\frac{1}{6}(p_{\pi\pi\mu}x_\nu - p_{\pi\pi\nu}x_\mu)\int_0^1 du e^{iup_{\pi\pi}\cdot x}\phi_{\pi\pi}^\sigma(u).\end{aligned}\quad (12)$$

The LCDA $\phi_{\pi\pi}$ is twist-2, and the other two are twist-3. Their normalisations are given as

$$\int_0^1 du\phi_{\pi\pi}^s(u) = \int_0^1 du\phi_{\pi\pi}^\sigma(u) = 1. \quad (13)$$

The conformal symmetry in QCD [55] indicates that the twist-3 LCDA have the asymptotic form [51–54]:

$$\phi_{\pi\pi}^s(u) = 1, \quad \phi_{\pi\pi}^\sigma(u) = 6u(1-u), \quad (14)$$

while the twist-2 LCDA can be expanded in terms of the Gegenbauer moments:

$$\phi_{\pi\pi}(u) = 6u(1-u)\sum_n a_n C_n^{3/2}(2u-1). \quad (15)$$

In most cases, contributions from higher Gegenbauer moments are suppressed and thus one may keep the lowest moment a_1 . It is worthwhile to stress that these LCDAs for a two-hadron system have the same form as the ones for a light scalar $\bar{q}q$ meson [51–54]. In Ref. [56], the first Gegenbauer moment for the $f_0(980)$ is calculated as ¹

$$a_1 = -1.35. \quad (16)$$

while the perturbative QCD analysis of the B_s decays has used a much smaller value [29]:

$$a_1 = -0.36. \quad (17)$$

III. HEAVY-TO-LIGHT FORM FACTORS

The $B_s \rightarrow \pi^+\pi^-$ transition can be parametrized by three form factors

$$\begin{aligned}\langle(\pi^+\pi^-)_S|\bar{s}\gamma_\mu\gamma_5 b|\bar{B}_s\rangle &= \frac{-i}{m_{B_s}}\left\{\left[P_\mu - \frac{m_{B_s}^2 - m_{\pi\pi}^2}{q^2}q_\mu\right]\mathcal{F}_1^{B_s\rightarrow\pi\pi}(m_{\pi\pi}^2, q^2) + \frac{m_{B_s}^2 - m_{\pi\pi}^2}{q^2}q_\mu\mathcal{F}_0^{B_s\rightarrow\pi\pi}(m_{\pi\pi}^2, q^2)\right\}, \\ \langle(\pi^+\pi^-)_S|\bar{s}\sigma_{\mu\nu}q^\nu\gamma_5 b|\bar{B}_s\rangle &= \frac{\mathcal{F}_T^{B_s\rightarrow\pi\pi}(m_{\pi\pi}^2, q^2)}{m_{B_s}(m_{B_s} + m_{\pi\pi})}\left[(m_{B_s}^2 - m_{\pi\pi}^2)q_\mu - q^2P_\mu\right],\end{aligned}\quad (18)$$

¹ In Ref. [56], the normalization factor for a scalar $\bar{q}q$ meson is $m_{f_0(980)}f_{f_0(980)}$, which is the $F_{\pi\pi}^s B_0$ in this work. The results for the twist-2 Gegenbauer moment in Eqs. (16) and (17) have been converted to our convention.

where the orbital angular momentum in the $\pi^+\pi^-$ system is chosen as zero in order to select the S-wave. The p_{B_s} and $p_{\pi\pi}$ is the momentum for the B_s and the $\pi\pi$ system, respectively. The momentum transfer is defined as $q = p_{B_s} - p_{\pi\pi}$, and the P_μ is defined as $P_\mu = p_{B_s} + p_{\pi\pi}$. Here the convention slightly differs with the ones adopted in Refs. [12–14]. The $D_s \rightarrow \pi^+\pi^-$ form factors can be analogously defined, with the replacement $m_{B_s} \rightarrow m_{D_s}$.

As we have demonstrated in Ref. [12], the LCSR allows us to express the $B_s \rightarrow \pi^+\pi^-$ form factors in terms of the $\pi^+\pi^-$ LCDAs [51–54, 57–59]. The LCSR factorization formulas read as [12],

$$\begin{aligned} \mathcal{F}_1^{B_s \rightarrow \pi\pi}(m_{\pi\pi}^2, q^2) &= N_F \left\{ \int_{u_0}^1 \frac{du}{u} \exp \left[-\frac{m_b^2 + u\bar{u}m_{\pi\pi}^2 - \bar{u}q^2}{uM^2} \right] \left[-\frac{m_b}{B_0} \Phi_{\pi\pi}(u) + u\Phi_{\pi\pi}^s(u) + \frac{1}{3} \Phi_{\pi\pi}^\sigma(u) \right. \right. \\ &\quad \left. \left. + \frac{m_b^2 + q^2 - u^2m_{\pi\pi}^2}{uM^2} \frac{\Phi_{\pi\pi}^\sigma(u)}{6} \right] + \exp \left[-\frac{s_0}{M^2} \right] \frac{\Phi_{\pi\pi}^\sigma(u_0)}{6} \frac{m_b^2 - u_0^2m_{\pi\pi}^2 + q^2}{m_b^2 + u_0^2m_{\pi\pi}^2 - q^2} \right\}, \end{aligned} \quad (19)$$

$$\begin{aligned} \mathcal{F}_-^{B_s \rightarrow \pi\pi}(m_{\pi\pi}^2, q^2) &= N_F \left\{ \int_{u_0}^1 \frac{du}{u} \exp \left[-\frac{m_b^2 + u\bar{u}m_{\pi\pi}^2 - \bar{u}q^2}{uM^2} \right] \left[\frac{m_b}{B_0} \Phi_{\pi\pi}(u) + (2-u)\Phi_{\pi\pi}^s(u) \right. \right. \\ &\quad \left. \left. + \frac{1-u}{3u} \Phi_{\pi\pi}^\sigma(u) - \frac{u(m_b^2 + q^2 - u^2m_{\pi\pi}^2) + 2(m_b^2 - q^2 + u^2m_{\pi\pi}^2)}{u^2M^2} \frac{\Phi_{\pi\pi}^\sigma(u)}{6} \right] \right. \\ &\quad \left. - \frac{u_0(m_b^2 + q^2 - u_0^2m_{\pi\pi}^2) + 2(m_b^2 - q^2 + u_0^2m_{\pi\pi}^2)}{u_0(m_b^2 + u_0^2m_{\pi\pi}^2 - q^2)} \exp \left[-\frac{s_0}{M^2} \right] \frac{\Phi_{\pi\pi}^\sigma(u_0)}{6} \right\}, \end{aligned} \quad (20)$$

$$\mathcal{F}_0^{B_s \rightarrow \pi\pi}(m_{\pi\pi}^2, q^2) = \mathcal{F}_1^{B_s \rightarrow \pi\pi}(m_{\pi\pi}^2, q^2) + \frac{q^2}{m_{B_s}^2 - m_{\pi\pi}^2} \mathcal{F}_-^{B_s \rightarrow \pi\pi}(m_{\pi\pi}^2, q^2), \quad (21)$$

$$\begin{aligned} \mathcal{F}_T^{B_s \rightarrow \pi\pi}(m_{\pi\pi}^2, q^2) &= 2N_F(m_{B_s} + m_{\pi\pi}) \left\{ \int_{u_0}^1 \frac{du}{u} \exp \left[-\frac{(m_b^2 - \bar{u}q^2 + u\bar{u}m_{\pi\pi}^2)}{uM^2} \right] \left[-\frac{\Phi_{\pi\pi}(u)}{2B_0} + m_b \frac{\Phi_{\pi\pi}^\sigma(u)}{6uM^2} \right] \right. \\ &\quad \left. + m_b \frac{\Phi_{\pi\pi}^\sigma(u_0)}{6} \frac{\exp[-s_0/M^2]}{m_b^2 - q^2 + u_0^2m_{\pi\pi}^2} \right\}, \end{aligned} \quad (22)$$

where

$$\begin{aligned} N_F &= B_0 F_{\pi\pi}^s(m_{\pi\pi}^2) \frac{m_b + m_s}{2m_{B_s} f_{B_s}} \exp \left[\frac{m_{B_s}^2}{M^2} \right], \\ u_0 &= \frac{m_{\pi\pi}^2 + q^2 - s_0 + \sqrt{(m_{\pi\pi}^2 + q^2 - s_0)^2 + 4m_{\pi\pi}^2(m_b^2 - q^2)}}{2m_{\pi\pi}^2}. \end{aligned} \quad (23)$$

In order to derive the above equations, the Borel transformation of hadronic and of QCD expressions of correlation functions has been carried out, defined as:

$$\mathcal{B}[\mathcal{F}(Q^2)] = \lim_{Q^2 \rightarrow \infty, n \rightarrow \infty, \frac{Q^2}{n} = M^2} \frac{1}{(n-1)!} (-Q^2)^n \left(\frac{d}{dQ^2} \right)^n \mathcal{F}(Q^2), \quad (24)$$

where \mathcal{F} is a function of $Q^2 = -q^2$ and M^2 is the Borel parameter. The explicit form is:

$$\mathcal{B} \left[\frac{1}{(s + Q^2)^n} \right] = \frac{\exp(-s/M^2)}{(M^2)^n (n-1)!}. \quad (25)$$

This operation improves the convergence of the OPE series by factorials of n and, for suitably chosen values of M^2 , enhances the contribution of the low-lying states to the correlation function.

For convenience we can define the normalized form factor:

$$\mathcal{F}_i(m_{\pi\pi}^2, q^2) = B_0 F_{\pi\pi}^s(m_{\pi\pi}^2) \bar{F}_i(q^2), \quad (26)$$

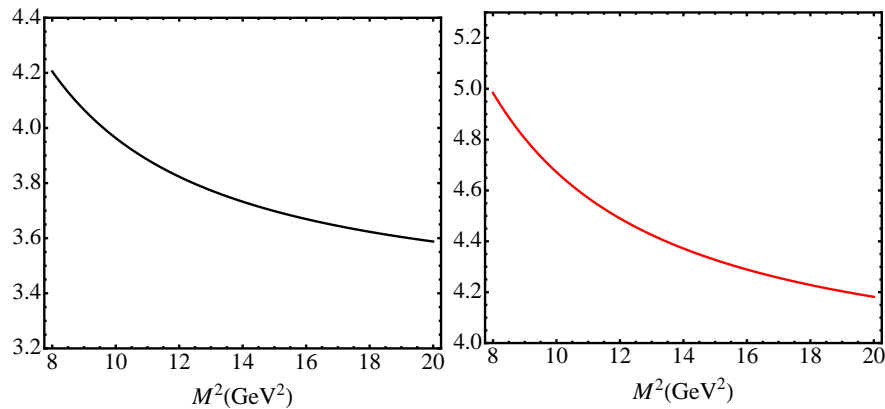


FIG. 3: At the maximal recoil $q^2 = 0$, the dependence of $\overline{F}_1(q^2 = 0) = \overline{F}_0(q^2 = 0)$ (left panel) and $\overline{F}_T(q^2 = 0)$ (right panel) on the Borel parameter M^2 . The final results are obtained requiring stability against variations of M^2 .

TABLE II: Fitted parameters of the $B_s/D_s \rightarrow \pi^+\pi^-$ form factors derived by LCSR.

$B_s \rightarrow \pi^+\pi^-$	$\overline{F}_i(q^2 = 0)$	a_i	b_i	$D_s \rightarrow \pi^+\pi^-$	$\overline{F}_i(q^2 = 0)$	a_i	b_i
\overline{F}_1	3.66	1.39	0.54	\overline{F}_1	2.45	0.82	0.20
\overline{F}_0	3.66	0.54	-0.08	\overline{F}_0	2.45	0.39	-0.15
\overline{F}_T	4.29	1.33	0.54				

where the $m_{\pi\pi}$ and q^2 dependence has been factorized into the $F_{\pi\pi}^s(m_{\pi\pi}^2)$ and $\overline{F}_i(q^2)$, respectively. This approximation is justified by the Watson-Madigan theorem [60, 61]. As a reference point, we will choose the $m_{\pi\pi} = m_{f_0(980)}$ to explore the functions $\overline{F}_i(q^2)$.

In the numerical analysis, we use [62, 63]

$$f_{B_s} = (224 \pm 5)\text{MeV}, \quad s_0 = (34 \pm 2)\text{GeV}^2, \quad B_0 = (1.7 \pm 0.2)\text{GeV}. \quad (27)$$

With these numerical inputs, the sum rules (19)-(22) provide us with the functions $\overline{F}_i(q^2)$ for each value of q^2 as a function of the Borel parameter. In Fig. 3, at $q^2 = 0$ we show the dependence on M^2 with $a_1 = -0.6$. The results are obtained requiring stability against variations of M^2 . As demonstrated in this figure, the form factors become stable when $M^2 > 12\text{GeV}^2$. The situations with different a_1 and q^2 values are similar and thus we can choose $M^2 = (16 \pm 2)\text{GeV}^2$.

Since the form factors are sensitive to the Gegenbauer moment a_1 of the twist-2 LCDA, in the left panel of Fig. 4 we show this dependence in the range $a_1 = (-1.4, -0.4)$ at the maximal recoil $q^2 = 0$. We will show later the value $a_1 = -0.6$ can describe well the data on both the $B_s \rightarrow \pi^+\pi^-\ell^+\ell^-$ and $D_s \rightarrow \pi^+\pi^-\ell\nu$.

The LCSR is applicable in the hard-scattering region. To access the momentum distribution in the full kinematics region, we will adopt the following parametrization

$$\overline{F}_i(q^2) = \frac{\overline{F}_i(0)}{1 - a_i q^2/m_{B_s}^2 + b_i (q^2/m_{B_s}^2)^2}, \quad (28)$$

where $i = 1, 0, T$. The parameters can be fitted in the region $q^2 < 5\text{GeV}^2$ for the B_s transition, and the results are collected in Tab. II.

For the $D_s \rightarrow \pi^+\pi^-$ transition, we use [63]

$$s_0 = (6.5 \pm 1)\text{GeV}^2, \quad f_{D_s} = (257.5 \pm 4.6)\text{MeV}, \quad m_c = 1.4\text{GeV}. \quad (29)$$

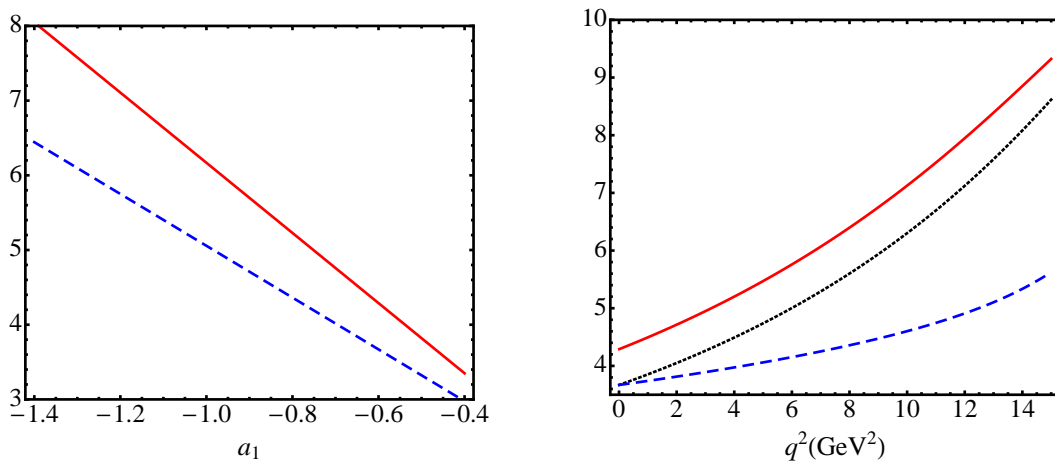


FIG. 4: At the maximal recoil $q^2 = 0$, the dependence of $\overline{F}_{1,0}$, and \overline{F}_T on the Gegenbauer moment a_1 is shown in the left panel. Dashed and solid curves correspond to $\overline{F}_1(q^2 = 0) = \overline{F}_0(q^2 = 0)$, and $\overline{F}_T(q^2 = 0)$, respectively. In the right panel, the q^2 dependence is given with $a_1 = -0.6$. Solid, dotted and dashed lines denote the $\overline{F}_T(q^2)$, $\overline{F}_1(q^2)$ and $\overline{F}_0(q^2)$, respectively.

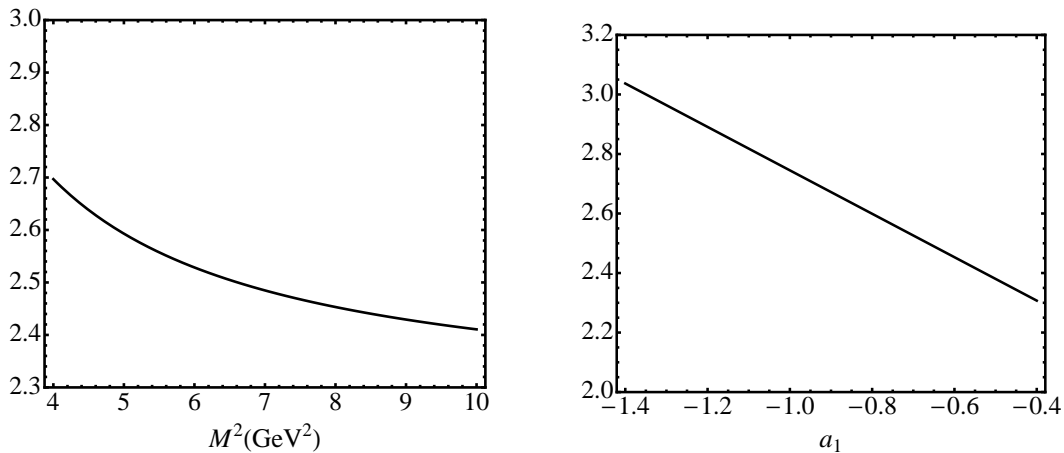


FIG. 5: The functions $\overline{F}_i(0)$ for the $D_s \rightarrow \pi^+\pi^-$: the dependence on M^2 (Gegenbauer moment a_1) in the left (right) panel.

The results for the $D_s \rightarrow \pi^+\pi^-$ form factors are given in Fig. 5. From the left panel, we can see the results are stable when $M^2 > 6\text{GeV}^2$, and we will use $M^2 = (8 \pm 1)\text{GeV}^2$. The dependence on the first Gegenbauer moment a_1 is less severe compared to the $B_s \rightarrow \pi^+\pi^-$ case, as shown in the right panel of Fig. 5. In the D_s mode, the twist-2 contributions in the regions with $x > 1/2$ and $x < 1/2$ cancel with each other. This fact has been explored in the study of $D_s \rightarrow f_0(980)$ transition [64]. Since the energy release in the D_s transition is small, we have used the $-5\text{GeV}^2 < q^2 < 0$ to fit the q^2 -dependent parameters in Eq.(28).

IV. PHENOMENOLOGICAL RESULTS

A. $B_s \rightarrow \pi^+ \pi^- \ell^+ \ell^-$

We proceed with the analysis of $B_s \rightarrow \pi^+ \pi^- \ell^+ \ell^-$, whose decay amplitude is governed by the effective Hamiltonian [65]

$$\mathcal{H}_{\text{eff}} = -\frac{G_F}{\sqrt{2}} V_{tb} V_{ts}^* \sum_{i=1}^{10} C_i(\mu) O_i(\mu).$$

The O_i is a four-quark or a magnetic-moment operator, and the $C_i(\mu)$ is its Wilson coefficient. The explicit forms can be found in Ref. [65]. G_F is the Fermi constant, and $V_{tb} = 0.99914 \pm 0.00005$ and $V_{ts} = -0.0405_{-0.012}^{+0.011}$ [63] are the CKM matrix elements. The bottom and strange quark masses are $m_b = (4.66 \pm 0.03) \text{ GeV}$ and $m_s = (0.095 \pm 0.005) \text{ GeV}$ [63].

In general, various partial-waves of two-hadron $M_1 M_2$ state contribute to a generic $B \rightarrow M_1 M_2 \ell^+ \ell^-$ process and the differential decay width has been derived using the helicity amplitude in Refs. [3–5]. In the $B_s \rightarrow \pi^+ \pi^- \mu^+ \mu^-$, the S-wave contribution dominate with the angular distribution:

$$\frac{d^3 \Gamma(B_s \rightarrow \pi^+ \pi^- \mu^+ \mu^-)}{dm_{\pi\pi}^2 dq^2 d \cos \theta_\ell} = \frac{3}{8} \left[J_1^c + J_2^c \cos(2\theta_\ell) \right], \quad (30)$$

where the coefficients are

$$J_1^c = |\mathcal{A}_{L0}^0|^2 + |\mathcal{A}_{R0}^0|^2 + 8\hat{m}_\ell^2 |\mathcal{A}_{L0}^0 \mathcal{A}_{R0}^{0*}| \cos(\delta_{L0}^0 - \delta_{R0}^0) + 4\hat{m}_\ell^2 |\mathcal{A}_t^0|^2, \quad (31)$$

$$J_2^c = -\beta_{2\ell}^2 \left\{ |\mathcal{A}_{L0}^0|^2 + |\mathcal{A}_{R0}^0|^2 \right\}. \quad (32)$$

In the above equations, $\beta_{2\ell} = \sqrt{1 - 4\hat{m}_\ell^2}$, $\hat{m}_\ell = m_\ell / \sqrt{q^2}$, and θ_ℓ is the polar angle between the B_s and the μ^- moving direction in the lepton pair rest-frame. The δ_{L0}^0 and δ_{R0}^0 are phases of the helicity amplitudes

$$\begin{aligned} \mathcal{A}_{L/R,0}^0 &= N_1^{2\ell} \sqrt{N_2^{2\ell}} i \frac{1}{m_{B_s}} \left[(C_9 \mp C_{10}) \frac{\sqrt{\lambda}}{\sqrt{q^2}} \mathcal{F}_1^{B_s \rightarrow \pi\pi}(q^2) + 2(C_{7L} - C_{7R}) \frac{\sqrt{\lambda} m_b}{\sqrt{q^2} (m_B + m_{\pi\pi})} \mathcal{F}_T^{B_s \rightarrow \pi\pi}(q^2) \right], \\ \mathcal{A}_{L/R,t}^0 &= N_1^{2\ell} \sqrt{N_2^{2\ell}} i \frac{1}{m_{B_s}} \left[(C_9 \mp C_{10}) \frac{m_{B_s}^2 - m_{\pi\pi}^2}{\sqrt{q^2}} \mathcal{F}_0^{B_s \rightarrow \pi\pi}(q^2) \right], \end{aligned} \quad (33)$$

$$\mathcal{A}_t^0 = \mathcal{A}_{R,t}^0 - \mathcal{A}_{L,t}^0 = 2N_1^{2\ell} \sqrt{N_2^{2\ell}} C_{10} i \frac{1}{m_{B_s}} \left[\frac{m_{B_s}^2 - m_{\pi\pi}^2}{\sqrt{q^2}} \mathcal{F}_0^{B_s \rightarrow \pi\pi}(q^2) \right]. \quad (34)$$

where

$$N_1^{2\ell} = \frac{G_F}{4\sqrt{2}} \frac{\alpha_{\text{em}}}{\pi} V_{tb} V_{ts}^* \quad (35)$$

$$N_2^{2\ell} = \frac{1}{16\pi^2} \sqrt{1 - 4m_\pi^2/m_{\pi\pi}^2} \times \frac{8}{3} \frac{\sqrt{\lambda} q^2 \beta_{2\ell}}{256\pi^3 m_{B_s}^3}. \quad (36)$$

The Källén function λ is related to the $\pi^+ \pi^-$ momentum in the B_s rest-frame:

$$\lambda \equiv \lambda(m_{B_s}^2, m_{\pi^+ \pi^-}^2, q^2), \quad \lambda(a, b, c) = a^2 + b^2 + c^2 - 2(ab + bc + ca). \quad (37)$$

In Fig. 6, results for differential branching fractions $d\mathcal{B}/dm_{\pi\pi}$ for the $B_s \rightarrow \pi^+ \pi^- \mu^+ \mu^-$ are given in panel (a) and (b), and the ones for $B_s \rightarrow \pi^+ \pi^- \tau^+ \tau^-$ are given in panel (c). The result in panel (a) clearly shows the peak corresponding to the $f_0(980)$. In order to compare with the experimental data [28], we also give the binned results in panel (b) in Fig. 6 from 0.5 GeV to 1.3 GeV with square markers. Dominant theoretical errors arise from the $B_0 = (1.7 \pm 0.2) \text{ GeV}$. The experimental data (with triangle markers) has been normalized to the central value

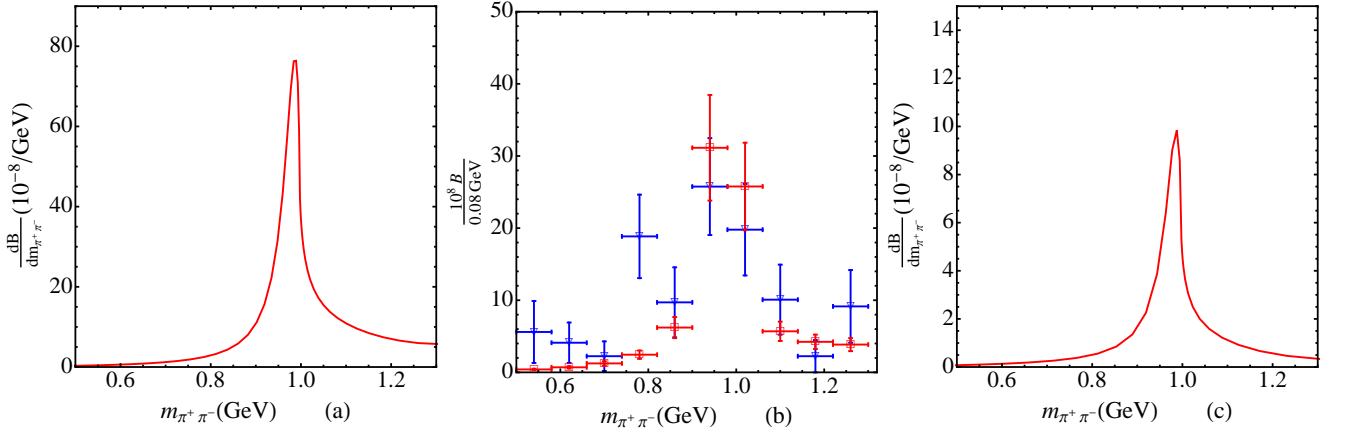


FIG. 6: Differential branching ratios $d\mathcal{B}/dm_{\pi\pi}$ for the $B_s \rightarrow \pi^+\pi^-\mu^+\mu^-$ in panel (a) and (b), and $B_s \rightarrow \pi^+\pi^-\tau^+\tau^-$ in panel (c). In panel (b), experimental data (with triangle markers) has been normalized to the central value of the branching fraction: $\mathcal{B}(B_s^0 \rightarrow \pi^+\pi^-\mu^+\mu^-) = (8.6 \pm 1.5 \pm 0.7 \pm 0.7) \times 10^{-8}$ [28], and theoretical results are shown with square markers.

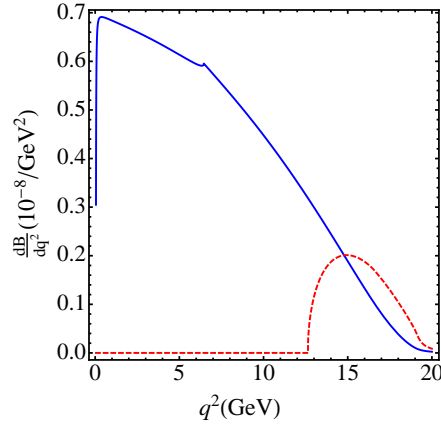


FIG. 7: The differential branching ratio $d\mathcal{B}/dq^2$ for the $B_s \rightarrow \pi^+\pi^-\mu^+\mu^-$ (solid curve) and $B_s \rightarrow \pi^+\pi^-\tau^+\tau^-$ (dashed curve) is given in unit of $10^{-8}/\text{GeV}^2$.

in Eq. (1). The comparison in this panel shows an overall agreement between our theoretical predictions and the experimental data. Integrating out the $m_{\pi\pi}$ from 0.5 GeV to 1.3 GeV, we have the branching fraction:

$$\mathcal{B}(B_s \rightarrow \pi^+\pi^-\mu^+\mu^-) = (6.9 \pm 1.6) \times 10^{-8}, \quad (38)$$

which is also consistent with the data in Eq. (2).

In Fig. 7, we predict the differential distribution $d\mathcal{B}/dq^2$ (in unit of $10^{-8}/\text{GeV}^2$) for the $B_s \rightarrow \pi^+\pi^-\mu^+\mu^-$ (solid curve) and for the $B_s \rightarrow \pi^+\pi^-\tau^+\tau^-$ (dashed curve). Results for the integrated branching fractions of $B_s \rightarrow \pi^+\pi^-\tau^+\tau^-$ are predicted as:

$$\mathcal{B}(B_s \rightarrow \pi^+\pi^-\tau^+\tau^-) = (8.8 \pm 2.1) \times 10^{-9}, \quad (39)$$

where $0.5\text{GeV} < m_{\pi\pi} < 1.3 \text{ GeV}$ is assumed. Our theoretical results could be examined at the future experimental facilities including the LHCb detector [66] and the Super-B factory at the KEK [67].

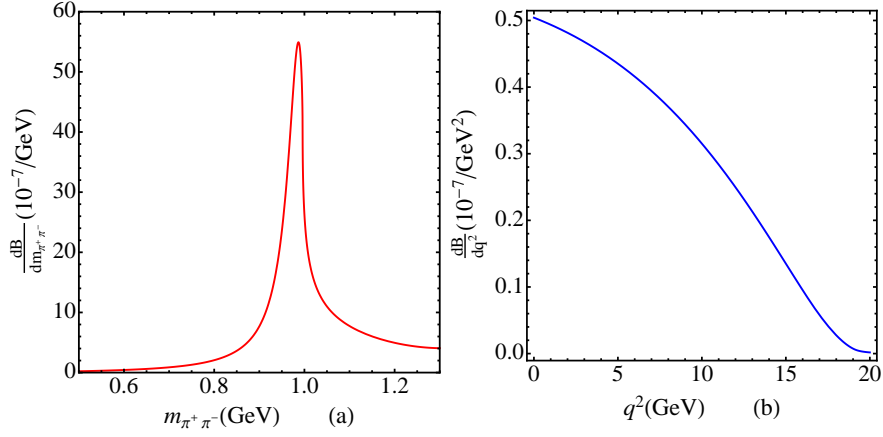


FIG. 8: The differential branching ratios for the $B_s \rightarrow \pi^+\pi^-\nu\bar{\nu}$: the left panel for the $d\mathcal{B}/dm_{\pi\pi}$, and the right one for the $d\mathcal{B}/dq^2$.

B. $B_s \rightarrow \pi^+\pi^-\nu\bar{\nu}$

The $b \rightarrow s\nu\bar{\nu}$ effective Hamiltonian is given by

$$\mathcal{H}_{b \rightarrow s\nu\bar{\nu}} = \frac{G_F}{\sqrt{2}} \frac{\alpha_{em}}{2\pi \sin^2(\theta_W)} V_{tb}V_{ts}^* \eta_X X(x_t) O_L \equiv C_L O_L, \quad (40)$$

which involves the four-fermion operator

$$O_L = [\bar{s}\gamma^\mu(1 - \gamma_5)b][\bar{\nu}\gamma_\mu(1 - \gamma_5)\nu]. \quad (41)$$

Here θ_W is the Weinberg angle; the function $X(x_t)$ ($x_t = m_t^2/m_W^2$, with m_t the top quark mass and m_W the W mass) has been computed in Refs. [65, 68], and the QCD factor η_X is found close to one [69–71].

With the above Hamiltonian, we obtain the differential decay width

$$\frac{d^2\Gamma(\bar{B}_s \rightarrow (\pi^+\pi^-)\nu\bar{\nu})}{dq^2 dm_{\pi\pi}^2} = 3 \times |A_0^0|^2, \quad (42)$$

where the factor 3 arises from three species of neutrinos. The helicity amplitude in this case is

$$A_0^0 = C_L \sqrt{N_2^\nu} i \frac{1}{m_{B_s}} \left[\frac{\sqrt{\lambda}}{\sqrt{q^2}} \mathcal{F}_1^{B_s \rightarrow \pi\pi}(m_{\pi\pi}^2, q^2) \right],$$

$$N_2^\nu = \frac{1}{16\pi^2} \sqrt{1 - 4m_\pi^2/m_{\pi\pi}^2} \times \frac{8}{3} \frac{\sqrt{\lambda} q^2}{256\pi^3 m_{B_s}^3}. \quad (43)$$

We give our predictions for the differential distributions for the $B_s \rightarrow \pi^+\pi^-\nu\bar{\nu}$ in Fig. 8: the left panel for the $d\mathcal{B}/dm_{\pi\pi}$, and the right one for the $d\mathcal{B}/dq^2$. The integrated branching fraction in the range $0.5\text{GeV} < m_{\pi\pi} < 1.3\text{GeV}$ is predicted as:

$$\mathcal{B}(B_s \rightarrow \pi^+\pi^-\nu\bar{\nu}) = (4.9 \pm 1.2) \times 10^{-7}. \quad (44)$$

There is a large chance measure this branching ratio at the Super-B factory at KEK [67].

C. $D_s \rightarrow \pi^+\pi^-\ell\nu$

The effective Hamiltonian for $c \rightarrow s\ell\nu$ transition is given as

$$\mathcal{H}_{c \rightarrow s\ell\nu} = N_1^\ell [\bar{s}\gamma_\mu(1 - \gamma_5)c][\bar{\nu}\gamma^\mu(1 - \gamma_5)\ell] + h.c., \quad (45)$$

with

$$N_1^\ell = \frac{G_F}{\sqrt{2}} V_{cs}. \quad (46)$$

The differential decay width for $D_s \rightarrow \pi^+\pi^-\ell\nu_\ell$ can be expressed as

$$\frac{d^3\Gamma}{dm_{K\pi}^2 dq^2 d\cos\theta_l} = \frac{3}{8} \left[I_1(q^2, m_{K\pi}^2) + I_2(q^2, m_{K\pi}^2) \cos(2\theta_l) + I_6 \cos(\theta_l) \right], \quad (47)$$

with the I_i having the form:

$$\begin{aligned} I_1(q^2, m_{\pi\pi}^2) &= [(1 + \hat{m}_l^2)|A_0^0|^2 + 2\hat{m}_l^2|A_t^0|^2], \\ I_2(q^2, m_{\pi\pi}^2) &= -\beta_l|A_0^0|^2, \\ I_6(q^2, m_{\pi\pi}^2) &= 4\hat{m}_l^2 \text{Re}[A_0^0 A_t^{0*}]. \end{aligned} \quad (48)$$

Using the $D_s \rightarrow \pi^+\pi^-$ form factors, the matrix element for D_s decays into the S-wave $\pi\pi$ final state is given as

$$\begin{aligned} A_0^0 &= N_1^\ell \sqrt{N_2^\ell} i \frac{1}{m_{D_s}} \left[\frac{\sqrt{\lambda}}{\sqrt{q^2}} \mathcal{F}_1^{D_s \rightarrow \pi\pi}(m_{\pi\pi}^2, q^2) \right], \\ A_t^0 &= N_1^\ell \sqrt{N_2^\ell} i \frac{1}{m_{D_s}} \left[\frac{m_{D_s}^2 - m_{\pi\pi}^2}{\sqrt{q^2}} \mathcal{F}_0^{D_s \rightarrow \pi\pi}(m_{\pi\pi}^2, q^2) \right], \end{aligned} \quad (49)$$

where

$$N_2^\ell = \frac{1}{16\pi^2} \sqrt{1 - 4m_\pi^2/m_{\pi\pi}^2} \times \frac{8}{3} \frac{\sqrt{\lambda} q^2 \beta_\ell}{256\pi^3 m_{D_s}^3}. \quad (50)$$

As discussed in Ref. [13], one can explore a number of the q^2 -dependent ratios and in particular the lepton flavor dependent ratio:

$$\mathcal{R}^{\mu/e}(m_{\pi\pi}^2, q^2) = \frac{d^2\Gamma(D_s \rightarrow \pi^+\pi^-\mu^+\nu_\mu)/dq^2 dm_{\pi\pi}^2}{d^2\Gamma(D_s \rightarrow \pi^+\pi^-e^+\nu_e)/dq^2 dm_{\pi\pi}^2}, \quad (51)$$

and the integrated form over q^2 :

$$R^{\mu/e}(m_{\pi\pi}^2) = \frac{d\Gamma(D_s \rightarrow \pi^+\pi^-\mu^+\nu_\mu)/dm_{\pi\pi}^2}{d\Gamma(D_s \rightarrow \pi^+\pi^-e^+\nu_e)/dm_{\pi\pi}^2}. \quad (52)$$

Our results are given in Fig. 9. The first panel corresponds to the $d\mathcal{B}/dm_{\pi\pi}$, in which the dotted and solid curves denote to the $D_s \rightarrow \pi^+\pi^-\mu\nu$ and $D_s \rightarrow \pi^+\pi^-e\nu$, respectively. One different behavior in the differential branching ratio with $B_s \rightarrow \pi^+\pi^-\ell^+\ell^-$ in the $m_{\pi\pi}$ distributions is the suppression in the large $m_{\pi\pi}$ region. The second panel shows the ratio $R^{\mu/e}(m_{\pi\pi}^2)$ defined in Eq. (52). A comparison with the experimental data on the differential branching fraction [31, 32] is given in panel (c), where we can also find the agreement.

The integrated branching fractions are predicted as

$$\mathcal{B}(D_s \rightarrow \pi^+\pi^-e^+\nu) = (1.52 \pm 0.36) \times 10^{-3}, \quad (53)$$

$$\mathcal{B}(D_s \rightarrow \pi^+\pi^-\mu^+\nu) = (1.68 \pm 0.39) \times 10^{-3}, \quad (54)$$

where $0.5\text{GeV} < m_{\pi\pi} < 1.3\text{GeV}$ has been adopted in the integration. Again the errors come from the QCD condensate parameter B_0 . Theoretical results are in good agreement with the CLEO results in Eqs. (3,4) [31–33]. We expect experimental errors will be greatly reduced since in future the BES-III collaboration will collect about $2fb^{-1}$ data in e^+e^- collision at the energy around 4.17GeV which will be used to study semileptonic and nonleptonic D_s decays [34].

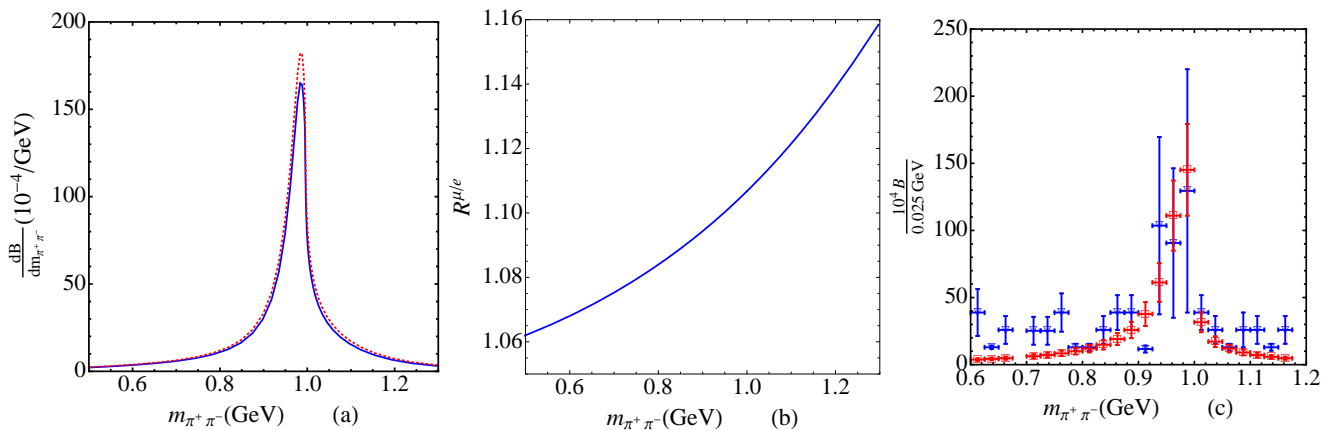


FIG. 9: The differential branching ratios for the $D_s \rightarrow \pi^+\pi^-\ell\nu$. The first panel corresponds to the $dB/dm_{\pi\pi}$, in which the dotted and solid curves correspond to $D_s \rightarrow \pi^+\pi^-\mu\nu$ and $D_s \rightarrow \pi^+\pi^-e\nu$ respectively. The second panel shows the ratio $R^{\mu/e}(m_{\pi\pi}^2)$ defined in Eq. (52). A comparison with the experimental data [31, 32] is given in panel (c).

V. CONCLUSIONS

Rare B decays have played an important role in testing the SM, and hunting for the NP. In recent years, a lot of experimental progresses have been made on the $B \rightarrow K^*\ell^+\ell^-$, and remarkably the LHCb collaboration has found a 3.7σ deviation from the SM for the ratio P_5' . This observable P_5' is believed almost independent on the hadronic uncertainties.

The analysis of $B \rightarrow V\ell^+\ell^-$, more appropriately $B \rightarrow M_1M_2\ell^+\ell^-$, requests not only the knowledge on the m_b expansion but also the M_1M_2 final state interactions. In this work, we have studied the $B_s^0 \rightarrow \pi^+\pi^-\ell^+\ell^-$, $B_s^0 \rightarrow \pi^+\pi^-\nu\bar{\nu}$ and $D_s^+ \rightarrow \pi^+\pi^-\ell^+\nu$ decay in the kinematics region where the $\pi^+\pi^-$ system has a invariant mass in the range 0.5-1.3 GeV. These processes are dominated by the S-wave contributions and thus they are valuable towards the determination of the S-wave $\pi^+\pi^-$ light-cone distribution amplitudes which are normalized to scalar form factors. We have compared the results for scalar form factors calculated in unitarized χ PT and the ones extracted from the data on the $B_s \rightarrow J/\psi\pi^+\pi^-$. We have derived the $B_s \rightarrow \pi^+\pi^-$ and $D_s \rightarrow \pi^+\pi^-$ transition form factor using the light-cone sum rules, and then presented our results for differential decay width which agree well with experimental data. Accurate measurements by the BES-III at the BEPC, the LHCb at the LHC and Super-B factory at KEKB in future will be valuable to more precisely examine our formalism, and determine the two-hadron LCDA.

Acknowledgements

The authors are grateful to Zhi-Hui Guo, Hsiang-Nan Li, Cai-Dian Lü, Ulf-G. Meißner, Wen-Fei Wang and Rui-Lin Zhu for enlightening discussions. This work was supported in part by Shanghai Natural Science Foundation under Grant No. 11DZ2260700 and No. 15ZR1423100, by the Open Project Program of State Key Laboratory of Theoretical Physics, Institute of Theoretical Physics, Chinese Academy of Sciences, China (No.Y5KF111CJ1), and by the Scientific Research Foundation for the Returned Overseas Chinese Scholars, State Education Ministry.

-
- [1] R. Aaij *et al.* [LHCb Collaboration], Phys. Rev. Lett. **111**, 191801 (2013) [arXiv:1308.1707 [hep-ex]].
 [2] The LHCb Collaboration [LHCb Collaboration], LHCb-CONF-2015-002, CERN-LHCb-CONF-2015-002.

- [3] C. D. Lu and W. Wang, Phys. Rev. D **85**, 034014 (2012) [arXiv:1111.1513 [hep-ph]].
- [4] B. Dey, arXiv:1505.02873 [hep-ex].
- [5] J. Gratrex, M. Hopfer and R. Zwicky, arXiv:1506.03970 [hep-ph].
- [6] D. Becirevic and A. Tayduganov, Nucl. Phys. B **868**, 368 (2013) [arXiv:1207.4004 [hep-ph]].
- [7] J. Matias, Phys. Rev. D **86**, 094024 (2012) [arXiv:1209.1525 [hep-ph]].
- [8] T. Blake, U. Egede and A. Shires, JHEP **1303**, 027 (2013) [arXiv:1210.5279 [hep-ph]].
- [9] D. Das, G. Hiller, M. Jung and A. Shires, JHEP **1409**, 109 (2014) [arXiv:1406.6681 [hep-ph]].
- [10] L. Hofer and J. Matias, arXiv:1502.00920 [hep-ph].
- [11] D. Das, G. Hiller and M. Jung, arXiv:1506.06699 [hep-ph].
- [12] U. G. Meiner and W. Wang, Phys. Lett. B **730**, 336 (2014) [arXiv:1312.3087 [hep-ph]].
- [13] U. G. Meiner and W. Wang, JHEP **1401**, 107 (2014) [arXiv:1311.5420 [hep-ph]].
- [14] M. Dring, U. G. Meiner and W. Wang, JHEP **1310**, 011 (2013) [arXiv:1307.0947 [hep-ph]].
- [15] W. Wang, Int. J. Mod. Phys. A **29**, 1430040 (2014) [arXiv:1407.6868 [hep-ph]].
- [16] S. Gardner and U. G. Meissner, Phys. Rev. D **65**, 094004 (2002) [hep-ph/0112281].
- [17] M. Maul, Eur. Phys. J. C **21**, 115 (2001) [hep-ph/0104078].
- [18] W. H. Liang and E. Oset, Phys. Lett. B **737**, 70 (2014) [arXiv:1406.7228 [hep-ph]].
- [19] M. Bayar, W. H. Liang and E. Oset, Phys. Rev. D **90**, 114004 (2014) [arXiv:1408.6920 [hep-ph]].
- [20] J. J. Xie and E. Oset, Phys. Rev. D **90**, 094006 (2014) [arXiv:1409.1341 [hep-ph]].
- [21] M. Sayahi and H. Mehraban, Phys. Scripta **88**, 035101 (2013).
- [22] T. Sekihara and E. Oset, arXiv:1507.02026 [hep-ph].
- [23] L. Roca, M. Mai, E. Oset and U. G. Meiner, Eur. Phys. J. C **75**, no. 5, 218 (2015) [arXiv:1503.02936 [hep-ph]].
- [24] C. H. Chen and H. n. Li, Phys. Lett. B **561**, 258 (2003) [hep-ph/0209043].
- [25] C. H. Chen and H. n. Li, Phys. Rev. D **70**, 054006 (2004) [hep-ph/0404097].
- [26] W. F. Wang, H. C. Hu, H. n. Li and C. D. L? Phys. Rev. D **89**, no. 7, 074031 (2014) [arXiv:1402.5280 [hep-ph]].
- [27] H. s. Wang, S. m. Liu, J. Cao, X. Liu and Z. j. Xiao, Nucl. Phys. A **930**, 117 (2014).
- [28] R. Aaij *et al.* [LHCb Collaboration], Phys. Lett. B **743**, 46 (2015) [arXiv:1412.6433 [hep-ex]].
- [29] W. F. Wang, H. n. Li, W. Wang and C. D. L? Phys. Rev. D **91**, no. 9, 094024 (2015) [arXiv:1502.05483 [hep-ph]].
- [30] W. Wang and R. L. Zhu, Phys. Lett. B **743**, 467 (2015) [arXiv:1502.05104 [hep-ph]].
- [31] J. Yelton *et al.* [CLEO Collaboration], Phys. Rev. D **80**, 052007 (2009) [arXiv:0903.0601 [hep-ex]].
- [32] K. M. Ecklund *et al.* [CLEO Collaboration], Phys. Rev. D **80**, 052009 (2009) [arXiv:0907.3201 [hep-ex]].
- [33] J. Hietala, D. Cronin-Hennessy, T. Pedlar and I. Shipsey, Phys. Rev. D **92**, no. 1, 012009 (2015) [arXiv:1505.04205 [hep-ex]].
- [34] D. M. Asner *et al.*, Int. J. Mod. Phys. A **24**, S1 (2009) [arXiv:0809.1869 [hep-ex]].
- [35] P. Colangelo and A. Khodjamirian, In *Shifman, M. (ed.): At the frontier of particle physics, vol. 3* 1495-1576 [hep-ph/0010175].
- [36] J. Gasser and U. G. Meissner, Nucl. Phys. B **357**, 90 (1991).
- [37] U. G. Meissner and J. A. Oller, Nucl. Phys. A **679**, 671 (2001) [hep-ph/0005253].
- [38] J. Bijnens and P. Talavera, Nucl. Phys. B **669**, 341 (2003) [hep-ph/0303103].
- [39] T. A. Lahde and U. G. Meissner, Phys. Rev. D **74**, 034021 (2006) [hep-ph/0606133].
- [40] Z. H. Guo, J. A. Oller and J. Ruiz de Elvira, Phys. Rev. D **86**, 054006 (2012) [arXiv:1206.4163 [hep-ph]].
- [41] J. Gasser and H. Leutwyler, Annals Phys. **158**, 142 (1984).
- [42] J. Gasser and H. Leutwyler, Nucl. Phys. B **250**, 465 (1985).
- [43] J. Gasser and H. Leutwyler, Nucl. Phys. B **250**, 517 (1985).
- [44] J. F. Donoghue, J. Gasser and H. Leutwyler, Nucl. Phys. B **343**, 341 (1990).
- [45] J. A. Oller, E. Oset and J. R. Pelaez, Phys. Rev. D **59**, 074001 (1999) [Phys. Rev. D **60**, 099906 (1999)] [Phys. Rev. D **75**, 099903 (2007)] [hep-ph/9804209].
- [46] M. Ablikim *et al.* [BES Collaboration], Phys. Lett. B **607**, 243 (2005) [hep-ex/0411001].
- [47] R. Aaij *et al.* [LHCb Collaboration], Phys. Rev. D **87**, no. 5, 052001 (2013) [arXiv:1301.5347 [hep-ex]].
- [48] R. Aaij *et al.* [LHCb Collaboration], Phys. Rev. D **89**, no. 9, 092006 (2014) [arXiv:1402.6248 [hep-ex]].
- [49] S. M. Flatte, Phys. Lett. B **63**, 224 (1976).
- [50] S. M. Flatte, Phys. Lett. B **63**, 228 (1976).
- [51] M. Diehl, T. Gousset, B. Pire and O. Teryaev, Phys. Rev. Lett. **81**, 1782 (1998) [hep-ph/9805380].

- [52] M. V. Polyakov, Nucl. Phys. B **555**, 231 (1999) [hep-ph/9809483].
- [53] N. Kivel, L. Mankiewicz and M. V. Polyakov, Phys. Lett. B **467**, 263 (1999) [hep-ph/9908334].
- [54] M. Diehl, Phys. Rept. **388**, 41 (2003) [hep-ph/0307382].
- [55] V. M. Braun, G. P. Korchemsky and D. Mueller, Prog. Part. Nucl. Phys. **51**, 311 (2003) [hep-ph/0306057].
- [56] H. Y. Cheng, C. K. Chua and K. C. Yang, Phys. Rev. D **73**, 014017 (2006) [hep-ph/0508104].
- [57] D. Miller, D. Robaschik, B. Geyer, F.-M. Dittes and J. Ho?eji, Fortsch. Phys. **42**, 101 (1994) [hep-ph/9812448].
- [58] P. Hagler, B. Pire, L. Szymanowski and O. V. Teryaev, Phys. Lett. B **535**, 117 (2002) [Phys. Lett. B **540**, 324 (2002)] [hep-ph/0202231].
- [59] B. Pire, F. Schwennsen, L. Szymanowski and S. Wallon, Phys. Rev. D **78**, 094009 (2008) [arXiv:0810.3817 [hep-ph]].
- [60] K. M. Watson, Phys. Rev. **88**, 1163 (1952).
- [61] A. B. Migdal, Sov. Phys. JETP, **1**, 2 (1955).
- [62] S. Aoki *et al.*, Eur. Phys. J. C **74**, 2890 (2014) [arXiv:1310.8555 [hep-lat]].
- [63] K. A. Olive *et al.* [Particle Data Group Collaboration], Chin. Phys. C **38**, 090001 (2014).
- [64] P. Colangelo, F. De Fazio and W. Wang, Phys. Rev. D **81**, 074001 (2010) [arXiv:1002.2880 [hep-ph]].
- [65] G. Buchalla, A. J. Buras and M. E. Lautenbacher, Rev. Mod. Phys. **68**, 1125 (1996) [hep-ph/9512380].
- [66] R. Aaij *et al.* [LHCb Collaboration], Eur. Phys. J. C **73**, no. 4, 2373 (2013) [arXiv:1208.3355 [hep-ex]].
- [67] T. Aushev *et al.*, arXiv:1002.5012 [hep-ex].
- [68] T. Inami and C. S. Lim, Prog. Theor. Phys. **65**, 297 (1981) [Prog. Theor. Phys. **65**, 1772 (1981)].
- [69] G. Buchalla and A. J. Buras, Nucl. Phys. B **400**, 225 (1993).
- [70] G. Buchalla and A. J. Buras, Nucl. Phys. B **548**, 309 (1999) [hep-ph/9901288].
- [71] M. Misiak and J. Urban, Phys. Lett. B **451**, 161 (1999) [hep-ph/9901278].